Author Manuscript

Author Manuscript

Author Manuscript

Author Manuscript

HHS Public Access

Author manuscript

Fuel (Lond). Author manuscript; available in PMC 2024 September 20.

Published in final edited form as:

Fuel (Lond). 2022 September 01; 323: . doi:10.1016/j.fuel.2022.124283.

Effects off hydrogenated vegetable oil (HVO) and HVO/biodiesel blends on the physicochemical and toxicological properties of emissions from an off-road heavy-duty diesel engine

Cavan McCaffery[a], **Hanwei Zhu**[a,b], **C. M. Sabbir Ahmed**[c], **Alexa Canchola**[c], **Jin Y. Chen**[c], **Chengguo Li**[b], **Kent C. Johnson**[a,b], **Thomas D. Durbin**[a,b], **Ying-Hsuan Lin**[c,d], **Georgios Karavalakis**[a,b,*]

[a]Bourns College of Engineering - Center for Environmental Research and Technology (CE-CERT), University of California, Riverside, CA 92507, United States

[b]Department of Chemical and Environmental Engineering, Bourns College of Engineering, University of California, Riverside, CA 92521, United States

[c]Environmental Toxicology Graduate Program, University of California, Riverside, CA 92521, United States

[d]Department of Environmental Sciences, University of California, Riverside, CA 92521, United States

Abstract

In this study, the regulated emissions, gaseous toxics, and the physical, chemical, and toxicological properties of particulate matter (PM) emissions from a legacy off-road diesel engine operated on hydrogenated vegetable oil (HVO) and HVO blends with biodiesel were investigated. This is one of the very few studies currently available examining the emissions and potential health effects of HVO and its blends with biodiesel from diesel engines. Extended testing was conducted over the nonroad transient cycle (NRTC) and the 5-mode D2 ISO 8718 cycle. Nitrogen oxide (NOx) emissions showed statistically significant reductions for HVO compared to diesel, whereas the biodiesel blends statistically significant increases in NOx emissions. PM and solid particle number reductions with pure HVO and the biodiesel blends were also observed. Low-molecular weight polycyclic aromatic hydrocarbons (PAHs) were the dominant species in the exhaust for all fuels, with pure HVO and the biodiesel blends showing lower concentrations of these pollutants compared to diesel fuel. Our results showed that the oxidative stress and cytotoxicity in PM emissions decreased with the use of biofuels. Notable correlations were observed between PM emissions and oxidative stress and cytotoxicity, especially elemental carbon and particle-phase PAH emissions.

Keywords

Hydrogenated vegetable oil; Biodiesel; NOx emissions; PAHs emissions; Toxicity

*Corresponding Author. gkaraval@cert.ucr.edu (G. Karavalakis).

Author Manuscript Author Manuscript Author Manuscript Author Manuscript

1. Introduction

On-road diesel engines for mobile sources have long being recognized as major sources of nitrogen oxides (NOx), particulate matter (PM), and other toxic pollutants [1–3]. Long-term exposures to emissions from diesel on-road engines, especially PM emissions, have been linked with adverse cardiovascular health implications, respiratory diseases, and higher hospitalization rates [4–5]. In an effort to reduce harmful emissions and improve air quality and health, on-road diesel engines have been subjected to strict emission regulations for controlling NOx and PM emissions. These regulations have led to the widespread adoption of selective catalytic reduction (SCR) systems and diesel particulate filters (DPFs) for the control of NOx and PM emissions, respectively. These efforts have resulted in about 90% and 75% less PM and NOx tailpipe emissions, respectively, from current on-road heavy-duty diesel vehicles equipped with robust aftertreatment systems compared to engine certified under the previous certification standards [6–8].

Less attention, on the other hand, has been paid to off-road engines and equipment used for construction, agricultural, port operation, and other applications, which are subjected to less stringent standards for controlling emissions. Since the emissions from catalyst-equipped on-road diesel engines have experienced dramatic reductions and are highly regulated, the relative contribution of older technology off-road diesel engines without aftertreatment systems has increased for NOx and PM emissions [9–11]. Estimates by the California Air Resources Board (CARB) shown that off-road engines, under the existing regulatory framework, are expected to contribute 95 tons per day (tpd) NOx, and 3.1 tpd of PM to the California emissions inventory in 2030, making off-road diesel engines the single largest source of mobile emissions in California. Currently, the Tier 4 final emission standards for off-road diesel engines necessitate the implementation of DPF and SCR systems to meet PM and NOx standards, respectively, although a significant engine population in California do not utilize robust exhaust aftertreatment controls. Future stringent standards (Tier 5) will likely include further NOx and PM emissions reductions from all new off-road diesel engines, as well as a possible first-time carbon dioxide (CO_2) emission standard. A number of studies have reported that heavy-duty diesel construction engines are significant sources of NOx and PM emissions and are characterized by their older age due to their longer life spans than highway engines [11–13].

While stricter emissions standards enforcing the implementation of DPF and SCR systems will result in important reductions in PM and NOx emissions, respectively, the adoption of alternative fuels can also provide a viable solution to reduce emissions from off-road diesel engines. Fatty acid methyl esters (FAME) or biodiesel, is the most popular biofuel for use in compression ignition (CI) engines. Biodiesel is an oxygenated fuel, free of sulfur and aromatic compounds, which can be produced from a range of vegetable oils, waste cooking oils, and animal fats via the transesterification reaction [14]. In engines without SCR, biodiesel has been shown to decrease emissions of carbon monoxide (CO), total hydrocarbons (THC), PM, black carbon, and accumulation mode particle number emissions, while a number of studies have shown an increase in NOx emissions with biodiesel [15–18]. Mueller et al. [19] suggested that biodiesel NOx increases can be attributed to a number of different factors that include shorter, more advanced combustion events, longer

Author Manuscript Author Manuscript Author Manuscript Author Manuscript

residence times, and higher peak temperatures, which are caused by air fuel ratios closer to stoichiometry for biodiesel. Other studies have also shown reductions in polycyclic aromatic hydrocarbon (PAH) and nitrated PAH emissions with biodiesel [20–23], but increases in carbonyl emissions [17, 20].

Hydrogenated vegetable oil (HVO) or renewable diesel has received considerable attention as a renewable drop-in fuel for CI applications [24–25]. HVO is a paraffinic fuel, free of sulfur and aromatics, produced from the hydrogenation of vegetable oils and animal fats, with a higher cetane number and lower density than petroleum diesel [25]. Many studies have shown reductions in NOx, CO, THC, and particle emissions with HVO use in highway heavy-duty engines without SCR [16, 26–28] and off-road diesel engines without SCR [29–30]. Available studies have overwhelmingly reported lower PAH emissions with HVO when compared to petroleum-derived diesel fuel [27, 31–33]. Murtonen et al. [31] and Westphal et al. [33] showed additional reductions in PAH emissions when oxygenated biodiesel fuel was blended into HVO. A different study, however, showed increases in PAH emissions for HVO compared to diesel fuel, but lower nitrated PAH emissions [34].

The present study evaluates the regulated and particulate emissions, gaseous air toxics, PAHs and nitrated PAH emissions, as well as the toxicological properties of PM from an off-road legacy diesel engine (an engine without SCR and DPF systems). With limited information available on the emissions characterization of HVO and biodiesel blends from off-road legacy diesel engines, where the benefits of these fuels might have greater impact due to these engines' less stringent emissions standards, this study provides important information about the potential benefits of these new fuels for reductions in wide range of pollutants. In addition, this work provides important information on the potential health effects of PM emissions from these fuels. Results for each pollutant are discussed as a function of fuel type and test cycle. The relationships of pollutant emissions with toxicological markers are also discussed.

2. Materials and Methods

2.1 Test engine and fuels

Testing was conducted on a legacy off-road diesel engine with no emissions aftertreatment controls. The test article was a 2009 John Deere in-line 4 cylinder, 4.5L engine with a power rating of 115 hp and meeting the Tier 3, 2004 emission standards. Table S1, Supplementary Material (SM), lists the main technical specifications of the test engine.

A total of four fuels were employed in this study, including a baseline CARB ultra-low sulfur diesel (ULSD), neat HVO (hereinafter denoted as R100), and two HVO-biodiesel blends at concentrations of R65/B35 (65% by volume HVO and 35% by volume biodiesel) and R50/B50. The diesel and renewable diesel fuels met the ASTM D975 requirements, with their main physicochemical properties listed in Table S2, (SM). The biodiesel fuel met ASTM D6751.

Author Manuscript Author Manuscript Author Manuscript Author Manuscript

2.2 Test cycles

Testing was performed over the nonroad transient cycle (NRTC) and the 5-mode D2 ISO 8718 cycle. The daily test sequence was performed as CCC B1B1B1 B2B2B2, B3B3B3 CCC B1B1B1, B2B2B2 B3B3B3 CCC, B1B1B1 CCC B3B3B3, CCC B2B2B2 CCC, respectively, over the five days of testing on each cycle, where 'C' is the baseline CARB ULSD, B1 is R100, B2 is R65/B35, and B3 is R50/B50. The NRTC is a transient test cycle used for the emission certification of off-road diesel engines developed by the US Environmental Protection Agency (EPA). The NRTC tests were run as hot-start tests with a 20-minute soak in between tests. A preconditioning test was run prior to any tests on a new fuel, or to the extent that the engine had cooled and was outside of the ordinary 20-minute soak. It should be noted that a modified version of the NRTC was utilized, as this engine was not designed to typically operate over such a duty cycle. For this modified NRTC, the engine speed (rpm) was held steady at the maximum rated speed, and then the engine was ramped through the torque profile for the NRTC. The ramped modal D2 cycle is a steady-state test used in engine certification for both highway and off-road engines. The D2 cycle was run as ramped modal cycle (RMC) with a sequence of steady-state modes with different weighting factors, as opposed to having each mode tested as a discrete mode. The D2 tests were run as hot stabilized tests warmed up prior to the start of the emissions test. The engine temperature was stabilized by bringing the engine to the first operating testing point load for about 250 seconds.

2.3 Emissions measurements and analysis

Emissions testing was performed at CE-CERT's Heavy-Duty Engine Dynamometer facility, consisting of a 600 hp General Electric DC electric engine dynamometer. Emissions measurements were obtained using CE-CERT's Mobile Emissions Laboratory [35]. Basic emissions measurements included THC, NOx, CO, CO_2, and PM mass. The gravimetric PM2.5 mass was collected on 47 mm diameter 2 μm pore Teflon filters (Whatman brand). The filters were measured for net gains from testing using a UMX2 ultra precision microbalance with buoyancy correction in accordance with the weighing procedure guidelines set forth in the Code of Federal Regulations (CFR). Real-time second-by-second particle size distributions between 5.6 to 560 nm were obtained using an Engine Exhaust Particle Sizer (EEPS) spectrometer (TSI 3090, firmware version 8.0.0). Particles were sampled at a flow rate of 10 L/min, which is considered to be high enough to minimize diffusional losses. They were then charged with a corona charger and sized based on their electrical mobility in an electrical field. Concentrations were determined through the use of multiple electrometers. Total particle number emissions were measured using a TSI 3776 ultrafine-Condensation Particle Counter (CPC) with a 2.5 nm cut point. The instrument operated at a flowrate of 1.5 L/min. Solid particle number emissions were measured according to the European Particle Measurement Programme (PMP) protocol using the AVL Particle Counter (APC plus) with a cut-off particle diameter of 23 nm.

Elemental carbon (EC), organic carbon (OC), metals, carbonyl compounds, PAHs, and nitro-PAHs were measured for both test cycles on all fuels with the exception of R65/B35 blend when tested on the D2 cycle. EC/OC fractions were collected on QAT Tissuquartz quartz-fiber filters (Pall-Gelman, Ann Arbor, MI, USA) that were pre-cleaned by firing

Author Manuscript Author Manuscript Author Manuscript Author Manuscript

for 5 hours at 600 °C to remove carbonaceous contaminants and the collected materials were subsequently quantified using a Thermal/Optical Carbon Aerosol Analyzer (Sunset Laboratory, Forest Grove, OR) according to NIOSH (National Institute of Occupational Safety and Health) Method 5040. PM-bound metals and trace elements were collected on 47 mm Teflon filters and analyzed using the X-Ray fluorescence (XRF) method, according to EPA IO-3.3. Carbonyl compounds (aldehydes and ketones) were sampled on 2,4-dinitrophenylhydrazine (DNPH) coated silica cartridges (Waters Corp., Milford, MA) from the secondary dilution tunnel using a mass flow controller to regulate the flow to 1 L/min through the cartridge. The DNPH cartridges were eluted with 2 mL of acetonitrile and analyzed with high-performance liquid chromatography (Waters 2690 Alliance System with 996 Photodiode Array Detector) following the US EPA TO-11 method.

Particulate-phase PAH samples were collected on Teflon-impregnated glass fiber (TIGF) filters (100 mm). Semi-volatile organic compounds (SVOC) or vapor-phase PAHs were collected using an Amberlite XAD-4 polyaromatic absorbent resin (Aldrich Chemical Company, Inc.). Samples were extracted separately for the semi-volatile and particle-PAHs with high-purity, high performance liquid chromatography (HPLC)-grade dichloromethane. The accelerated solvent extraction (ASE) method was used for extraction, where the media were put in an cell for 15 min at 1500 psi and 80 °C. Deuterated internal standards that were added prior to extraction for both the XAD and filters included: naphthalene-d_8, acenaphthylene-d_8, phenanthrene-d_{10}, anthracene-d_{10}, chrysene-d_{12}, pyrene-d_{10}, benz[a]anthracene-d_{12}, benzo[a]pyrene-d_{12}, benzo[e]pyrene-d_{12}, benzo[k]fluoranthene-d-$_{12,}$ benzo[g,h,i]perylene-d_{12}, and coronene-d_{12}. Extracts were vacuum concentrated at 35–45 °C by rotary evaporation to ~1 mL, and filtered with a disposable 0.2 μm PTFE filter (Whatman Pura disc TM 25TF). The filtrate volume, including the flask rinse with solvent, was ~4 mL, to which ~500 μl of hexane was added. This mixture was then reduced to ~250 μL using a gentle stream of ultra-high purity (UHP) nitrogen (with a Chrompack CP-Gas-Clean moisture filter). Electron impact (EI) gas chromatography-mass spectrometry (GC-MS) by selective ion monitoring (SIM) using a CP-8400 autosampler equipped Varian 4000 GC-MS with a 30-m 5% phenylmethylsilicone fused-silica capillary column (DB-5MS+DG, J&W Scientific, Folsom CA) was used to analyze the XAD extracts. Filter-based PAHs were analyzed with a Scion 456 GC interfaced with a Scion TQ triple quadrupole MS/MS and equipped with CP-8400 autosampler with the same capillary column described above. For each compound quantified, a 6-level calibration a mid-level check was done at least once every ten samples.

2.4 Toxicology analysis

The 47 mm Teflon filters were extracted with 20 mL of methanol followed by 50 min of sonication. After sonication, the extracted filters were removed from the vial and the extracted solutions were used for the analyses of PM oxidative potential and subsequent cell exposures. For the dithiothreitol (DTT) assay, testing on all PM samples was carried out in 96-well plates (Greiner Bio-One, clear flat bottom) using protocols modified from previous studies [36]. DTT (5 mM) and 5–5'-dithiobis (2-nitrobenzoic acid) or DTNB (10 mM) stock solutions were prepared in KH_2PO_4 buffer (pH 7.4) and methanol, respectively. The stock solutions were diluted in the buffer to make working solutions of DTT (0.5

Author Manuscript Author Manuscript Author Manuscript Author Manuscript

mM) and DTNB (1 mM). Each fuel reaction mixture in the 96-well plate consisted of 50 μL buffer, 70 μL (1 μg) of the fuel sample, and 5 μL of 0.5 mM DTT, and incubated at 37 °C for three incubation periods of 30, 90, and 120 min. After each incubation period, 10 μL of 1 mM DTNB was added into the mixture to titrate the remaining DTT to form 2-nitro-5-thiobenzoic acid (TNB), whose absorbance was measured with a microplate reader (TECAN SpectraFluor Plus) at absorbance/reference wavelengths of 405/620 nm. The final reaction volume for each well was 135 μL, and each fuel sample was tested in triplicate. To determine DTT consumption rate of fuel samples, a calibration using different DTT concentrations (0 to 5 μL of 0.5 mM DTT) were carried out in reaction mixtures with 55 μL buffer, 70 μL methanol, and 10 μL of 1 mM DTNB. The final DTT consumption rates of the test fuels were derived from the slope of y=mx + b, which the LINEST function was applied to set the constant b as zero.

Human airway epithelial cells (BEAS-2B) were obtained from the American Type Culture Collection (ATCC). Cells were cultured in Gibco® LHC-9 medium (1×) (Invitrogen) grown at 37 °C and 5% CO_2 in a humidified incubator. Cells were cultured in T-75 flasks at a density of 3×10^5 cells/flask. The cell medium was replaced every 48 hours. Upon 80–90% confluency, cells were harvested using phosphate-buffered saline (PBS) for washing and incubated with 4 mL of 0.25% trypsin EDTA/PBS for 4 min at 37 °C to allow detachment.

Cells were seeded in 24-well plates at a density of 2.5×10^4 cells per well in 250 μL of LHC-9 medium for 48 hours prior to exposure. After the exposure time, cells reached around 60–70% confluence. PM extracts were dried off under a gentle nitrogen stream and reconstituted with the LHC-9 medium. Cells were washed with phosphate buffered saline (PBS) and then exposed to 50 μg/mL of PM extracts in the LHC-9 medium for 24 h. Experiments were conducted in triplicate per treatment group.

Cells were seeded in 96-well plates at a density of 5×10^3 cells per well in 100 μL of LHC-9 medium for 48 hours prior to exposure for cytotoxicity assay. Supernatants were collected 24 h after exposure. The CytoTox-ONE™ homogeneous membrane integrity assay protocol (Promega) was used to measure the cell membrane integrity and cell cytotoxicity. Triton X-100 (0.1%) was used as a positive control to simulate 100% cell death. The fluorescence for LDH assay (excitation 560/emission 585 nm) was measured using a TECAN SpectraFluor Plus microplate reader.

After 24 hours of exposure, cells were lysed with 350 μL of cold TRI Reagent (Zymo Research) for the total RNA extraction. Using the spin column-based Direct-zol RNA MiniPrep kit (Zymo Research), extracted RNA samples were further purified. RNA quality and concentrations were determined using a NanodropND-1000 spectrophotometer (Thermo Fisher Scientific). Isolated RNA samples were stored at −80 °C until processing.

Selected biomarkers, including Cytochrome P450 Family 1 Subfamily A Member 1 (CYP1A1), hemeoxygenase 1 (HMOX-1), tumor necrosis factor-alpha (TNF-α), were measured using the one-step QuantiFast SYBR Green® RT-PCR kit (Qiagen). The QuantiTect Primer Assays (Qiagen) of CYP1A1, HMOX-1, and TNF-α were used in this study. Results were normalized to a housekeeping gene beta-actin (ACTB) and expressed

Author Manuscript Author Manuscript Author Manuscript Author Manuscript

as $\log_2$ fold changes over the unexposed controls. Thermal cycling conditions for RT-PCR were set as follows: 10 min at 50 °C for reverse transcription, 5 min at 95 °C for initial denaturation, and 40 cycles of amplification (10 s at 95 °C and 30 s at 60 °C).

3. Results and Discussion

3.1 NOx Emissions

Figure 1 shows the average NOx emissions for each fuel and test cycle in g/bhp-hr. R100 resulted in the lowest NOx emissions compared to CARB ULSD and the biofuel blends for both test cycles. R100 showed statistically significant reductions in NOx emissions of 5.4% for the NRTC cycle and 4.9% for the D2 cycle compared to CARB ULSD. The R65/B35 did not show any statistically significant differences compared to CARB ULSD for either the NRTC or D2 cycles, while the R50/B50 blend showed statistically significant increases of 1.8% for the NRTC and 4.2% for the D2 cycle compared to CARB ULSD. Our results agree with those reported lower NOx emissions with HVO and higher NOx with biodiesel compared to diesel fuel [15–16, 18–19, 27–28]. The lower NOx emissions with R100 can be ascribed to the absence of aromatics in the fuel. Aromatic fuels have higher stoichiometric adiabatic flame temperature than paraffinic fuels, leading to higher combustion temperatures and greater formation of thermal NOx [37]. In addition, the higher cetane number of R100 compared to CARB ULSD likely reduced the fraction of fuel burnt during the premixed phase of the combustion event and thus NOx formation [26–27]. Other studies have also highlighted the importance of the injection control strategy on the observed NOx differences between HVO and diesel fuel, which is particularly true for older technology diesel engines where larger NOx reductions occur with HVO, similar to the current study [24]. The higher NOx emissions for the R50/B50 blend were likely due to the presence of oxygen atoms to the functional group of biodiesel, which increase the ignition delay period, resulting in higher in-cylinder temperatures and higher levels of thermal NOx [19, 38].

3.2 Particulate Emissions

Figure 2a shows the average gravimetric PM mass emissions and PM speciation (EC/OC fractions). PM mass emissions showed large statistically significant decreases for R100 and the biodiesel blends for both test cycles. The reductions for the NRTC compared to CARB ULSD were 38% for R100, 53% for R65/B35, and 63% for R50/B50. The reductions for the D2 cycle compared to CARB ULSD were 27% for R100, 51% for R65/B35, and 58% for R50/B50. Emissions of OC were comparable between the CARB ULSD and R100, and the biodiesel blends within the experimental variability, with the exception of the R50/B50 blend over the NRTC, which showed a statistically significant reduction of 46%. EC emissions showed larger reductions for the biofuel blends when compared to CARB ULSD. R100 showed marginally statistically significant reductions in EC emissions of 14% for the D2 cycle and 28% for the NRTC compared to CARB ULSD. Both biodiesel blends showed statistically significant reductions in EC emissions ranging from 58% to 68% compared to CARB ULSD over both cycles.

Figure 2b shows the total and solid particle number emissions for both test cycles. Overall, the use of R100 and the biodiesel blends provided statistically significant reductions in total

Author Manuscript Author Manuscript Author Manuscript Author Manuscript

particle number and solid particle number above 23 nm in diameter compared to CARB ULSD. An exception was seen for R100 over the D2 cycle (14%), with relatively large variability though as indicated by the wider error bars. The biodiesel blends led to the largest reductions in total and solid particle number emissions compared to CARB ULSD and R100, which is consistent with the PM mass trends for this engine. For the D2 cycle, these reductions ranged from 47%−50% for total particle number and from 21%−40% for solid particle number. For the NRTC, the reductions ranged from 16%−43% for total particle number and from 19%−48% for solid particle number.

PM mass and particle number emissions reductions have been shown in previous studies with biodiesel and HVO fuels [15–17, 21, 27, 31, 34, 39]. The reductions in particulate emissions for R100 can be attributed to the absence of aromatics and sulfur compounds, which can act as soot precursors. In addition, the narrow distillation profile of R100 and the lower T90 temperature (less heavy hydrocarbon fractions) will lead to better evaporation characteristics and reduced soot formation rates. The particulate reductions with the biodiesel blends were a consequence of the fuel-bound oxygen in methyl ester molecule, which possibly contributed to higher in-cylinder temperatures and better soot oxidation. The presence of oxygen can also reduce the fuel rich zones where diffusive combustion occurs, effectively reducing soot nucleation [17, 38]. An earlier study proposed that the higher oxygen availability in the fuel will allow more of the carbon to be oxidized to CO, thereby removing it from soot-precursor reactions [40]

The average particle size distributions are shown in Figure 3. Overall, both test cycles exhibited a bimodal particle size distribution. The NRTC showed higher particle populations for all fuels compared to the D2 cycle due to the transient nature of this cycle. For the NRTC, the concentrations of accumulation mode particles, mainly consisting of soot agglomerates, for all fuels were higher than those in the nucleation mode. The use of R100 and the biodiesel blends provided lower concentrations of accumulation mode particles, consistent with the PM mass results. It is interesting to note the multi-peak profile of CARB ULSD in the accumulation mode, peaking at 60 nm and 165 nm. This is in line with the higher PM mass and EC emissions for CARB ULSD over the NRTC compared to D2 cycle, and the higher emissions for this fuel compared to R100 and the biodiesel blends. Similar trends were observed for the D2 cycle, although the R100 showed higher concentrations of accumulation mode particles than CARB ULSD, but at smaller sizes (45 nm vs. 60 nm). For both cycles, the biodiesel blends showed considerably lower accumulation mode particles than CARB ULSD and R100, ranging from 40–45 nm in diameter. Despite the lack of aromatics and sulfur species in R100, the oxygen effect was much stronger in suppressing soot formation, leading to the better oxidation of soot particles, as well as to the reduced soot formation from the C=O bond. It is worth noting that the biodiesel blends over the NRTC exhibited higher populations of nucleation mode particles in the 10 nm range than the CARB ULSD and R100. This phenomenon could be due to the oxygen content of biodiesel that caused carbonaceous particles to change from the ultrafine size to the nanoparticle size, as well as to the higher viscosity and lower volatility of biodiesel blends (as shown in Table S2, SM), which resulted in poor fuel evaporation and imperfect mixing with air in the combustion chamber, leading in an increase of soluble organic fraction emissions and the generation of nucleation mode particles [41].

Author Manuscript Author Manuscript Author Manuscript Author Manuscript

3.3 Carbonyl compounds emissions

Carbonyl emissions are presented in Figure 4. Formaldehyde and acetaldehyde were the dominant aldehydes in the exhaust for all fuels and both cycles, followed by acrolein, acetone, MEK/butyraldehyde, propionaldehyde, and valeraldehyde. Previous studies have also shown the predominance of the low molecular weight formaldehyde and acetaldehyde emissions in diesel exhaust, primarily formed in the combustion process from fuel fragments produced in the initial fuel pyrolysis [17, 21, 33–34]. No statistically significant differences were seen between R100 and R65/B35 fuels compared to CARB ULSD for either the NRTC or D2 cycles. On the other hand, R50/B50 showed statistically significant reductions for most carbonyl emissions, including formaldehyde, acetaldehyde, and acrolein, over both cycles when compared to CARB ULSD. The results reported here are in contrast with many published studies that have reported increases in carbonyl emissions with biodiesel due to the presence of oxygen in the ester group [17, 20, 34], but in agreement with other studies demonstrating reductions in carbonyl emissions with biodiesel [21, 42]. Carbonyl emissions showed upward trends with R100 compared to CARB ULSD, especially for the D2 cycle, with the larger increases observed for propionaldehyde, MEK, valeraldehyde, and hexanaldehyde. Increases for R100 relative to CARB ULSD were also seen for the same compounds over the NRTC, but not at a statistically significant level. Although paraffinic fuels tend to decrease carbonyls formation [43], earlier works have also reported higher carbonyl emissions with HVO compared to diesel fuel [27].

3.4 Trace elements and metals emissions

Metals and trace elements concentrations in the PM are shown in Table 1. Many of the trace elements and metals were below the uncertainty levels of the test method and are not included in the analysis. Overall, metals and elements were seen in higher levels for the more transient NRTC than the steady-state D2 cycle, similar to the PM mass trends. Sodium (Na), sulfur (S), chlorine (Cl), and zinc (Zn) were the dominant species in the PM, followed by calcium (Ca), iron (Fe), and phosphorus (P). Iron and S can be sourced from both the fuel and lubricant oil, whereas Fe, Cu, and Si can be sourced from engine wear due to abrasion from metallic surfaces (i.e., piston rings, valves, etc.). Species such as Na, Ca, and Zn could be originated from the lubricant oil, since they exist in the lubricant oil additive package. Consistent with previous studies, R100 and biodiesel blends showed some reductions in PM-bound metals and elements emissions compared to CARB ULSD [21, 23].

3.5 PAH and nitro-PAH emissions

Figure 5 shows the sum of the vapor- and particle-phase substituted, phenyl- non-substituted, oxygenated (oxy), and total PAH emissions for all fuels over the NRTC and D2 cycles. Table S3 and Table S4 (SM) list all individual PAH species in the vapor- and particle-phase, respectively. Clearly, the vapor-phase PAHs showed significantly higher concentrations than those in the particle-phase. For the vapor-phase PAHs, the ethyl- and methyl-substituted and non-substituted PAHs were the largest contributors to the vapor-phase emissions, with the phenyl and oxy-PAHs showing very low concentrations. The light molecular weight species with two aromatic rings, such as naphthalene and methyl- and dimethyl-naphthalenes were the dominant vapor-phase PAHs. PAHs with three or more rings, such as

Author Manuscript Author Manuscript Author Manuscript Author Manuscript

phenanthrene, were seen in considerably lower concentrations, while heavier PAHs, which are absorbed onto PM due to their lower vapor pressure, were practically not detected. Some lighter two-ring oxy-PAHs were also detected in the vapor-phase, including 9-fluorenone and 1,4-naphthaquinone. Oxy-PAHs and quinones in particular are of toxicological and mutagenic interest because of their ability to generate reactive oxygen species (ROS) and pro-inflammatory effects [44–45]. For the particle-phase PAHs, oxy-PAHs comprising mainly of 1,8-naphthalic anhydride, 9-fluorenone, acenaphthenequinone, perinaphthenone, anthraquinone, 4-biphenylcarboxyaldehyde, and benzanthrone were the dominant species in the particle-phase emissions followed by the non-substituted and substituted PAHs. While polycyclic aromatic quinones in PM emissions have been reported to be present mostly in the vapor-phase [44], several of these species were found in the particle-phase and in even higher concentrations than those of benzo(a)pyrene.

The results for the 16 EPA priority particle-phase PAH emissions showed that phenanthrene and fluoranthene were the predominant species, followed by naphthalene, chrysene, and benzo(k)fluoranthene. Benzo(a)pyrene, a compound classified as human carcinogen by the International Agency for Research on Cancer (IARC), was not detectable for the D2 cycle and was seen in low concentrations for the NRTC. High molecular weight species with five and six aromatic rings, such as perylene, indeno[123-c,d]pyrene, and dibenzo(a,h)anthracene were almost undetectable. For the vapor-phase 16 EPA priority PAHs, naphthalene was by far the dominant compound, followed by acenaphthylene and phenanthrene. Previous works have also reported on the dominance of lighter PAHs in diesel exhaust [21, 46–47]. The lighter PAHs in the exhaust were a consequence of the incomplete combustion of fuel fragments and lubricant oil through pyrolysis and pyrosynthesis processes [48].

The use of R100 and its blends with biodiesel resulted in significant reductions in both vapor- and particle-phase PAH emissions. For the NRTC, the reductions in particle-phase PAHs were 28% for R100, 63% for R65/B35, and 72% for R50/B50, while the reductions in vapor-phase PAHs were 82% for R100, 88% for R65/B35, and 92% for R50/B50. For the D2 cycle, the reductions in particle-phase PAHs were 74% for R100 and 52% for R50/B50, while the reductions in vapor-phase PAHs were 96% for R100 and 88% for R50/B50. Consistent with previous studies that utilized biodiesel and HVO, the reductions in PAH emissions were due to the absence of aromatics and PAH species in both the methyl ester and the HVO [20–21, 27, 31, 33]. It is therefore reasonable to assume that the majority of these emissions would originate from pyrosynthesis pathways of lower molecular weight hydrocarbons in the fuel. The lower PAH emissions with increasing biodiesel were likely due to the combined effect of the higher oxygen content and the absence of aromatics. In an earlier study, Karavalakis et al [49] suggested that PAH formation from biodiesel combustion involves the formation of cyclic alkenes via the Diels-Alder reaction and their subsequent dehydrogenation to generate aromatic compounds.

Out of the 35 nitro-PAHs analyzed, only five nitro-PAHs were detected in the particle-phase and two in the vapor-phase (Table S5, SM). Similar to previous works, nitro-PAH emissions were found to be orders of magnitude lower than their parent PAHs [46–47, 49]. The three-ring species of 3-nitrophenanthrene and 2-nitrofluoranthene dominated the particle-phase emissions, followed by the two-ring 2-nitronapthalene and the four-ring 6-nitrochrysene and

Author Manuscript Author Manuscript Author Manuscript Author Manuscript

1-nitropyrene. The two-ring 1-nitronaphthalene and 2-nitronaphthalene were only detected in the vapor-phase, with 2-nitrofluorene being detected only for CARB ULSD. Overall, nitro-PAH emissions did not show any consistent trends between the fuels, with the results showing relatively large variability.

3.6 PM toxicological properties

Figure 6 (a–c) summarizes the toxicological properties of the PM extracts obtained from each fuel over both test cycles. Overall, the PM emissions from all test fuels demonstrated DTT activity (Figure 6a), indicating their potential to induce oxidative damage when exposed to a cellular system [50]. DTT activity was found to be greatest for CARB ULSD over both test cycles (0.00131 and 0.00147 nmol/min/μg, respectively). Compared to CARB ULSD, the reductions for the NRTC in oxidative activity were 71.3% for R100, 54.3% for R65/B35, and 72.7% for R50/B50, whereas for the D2 cycle these reductions were 63.5% and 45.9% for R100 and R50/B50, respectively. Previous studies have also reported lower DTT activities for biodiesel blends and/or HVO compared to petroleum diesel fuel [21, 51–53]. The presence of oxygen for the biodiesel blends and the lack of aromatics for all biofuels were likely the main factors for their lower DTT activity compared to CARB ULSD, as the presence of more redox-active hydrocarbon species (e.g., perinaphthenone and acenaphthenequinone) led to the formation of ROS (e.g., superoxide, HOOH, and OH) that can oxidize DTT.

The cytotoxicity of the PM extracts from each test fuel was assessed using the lactate dehydrogenase (LDH) assay to measure cell membrane integrity of human airway epithelial cells (BEAS-2B) after 24 hours of exposure to the PM extracts (Figure 6b). For the NRTC, CARB ULSD demonstrated significantly greater cytotoxicity to exposed BEAS-2B cells compared to the biodiesel blends and R100, and CARB ULSD over the D2 cycle. The lowest cytotoxicity that was seen for the biodiesel blends relative to R100, suggests that the oxygenated methyl ester fraction in the biodiesel blends will likely contribute to PM constituents of lower toxicity, such as PAHs. Previous studies have also reported that HVO and biodiesel blends generally induce lower cytotoxicity than diesel fuel due to their lower total PAH emissions [22, 53–54]. Overall, cytotoxicity was found to be below 30% for all fuels, indicating that the cells are stressed after 24-hour exposure, but the concentrations are not overly toxic to the point where further gene expression analysis was necessary [55]. For this reason, 50 μg/mL of each PM extract was chosen as the exposure concentration for subsequent analysis.

Figure 6c shows the relative gene expression levels of CYP1A1, HMOX-1, and TNF-α after exposure of BEAS-2B cells to PM emission extracts. Gene expression levels are expressed as log change (Log_2) over the unexposed control and were calculated using the comparative cycle threshold ($2^{-\Delta\Delta CT}$) method [56]. HMOX-1 demonstrated consistent upregulation, with exposure to PM extracts from the R50/B50 blend over the D2 cycle resulting in the greatest expression. HMOX-1 is commonly used as a biomarker of oxidative injury as gene expression can induced by chemical and physical agents that generate ROS [57]. Observed upregulation of HMOX-1 indicates that oxidative stress and injury to cells has occurred after 24-hour exposure. The increased upregulation seen in cells exposed to

Author Manuscript Author Manuscript Author Manuscript Author Manuscript

the R50/B50 blend over the D2 cycle contrasts with our observed DTT results, which indicated this fuel as having the lowest oxidative potential of all test fuels. CYP1A1 was also found to be upregulated after exposure to CARB ULSD and R50/B50 over the D2 cycle, as well as R65/B35 over the NRTC. Exposure to the R50/B50 blend over the NRTC, however, resulted in a downregulation of CYP1A1. CYP1A1 is a phase I metabolic enzyme that has been previously suggested to play an oncogenic role in various cancers, as it is known to play a key role in the bioactivation of PAHs, such as benzo[a]pyrene, to carcinogenic epoxide forms [58]. As such, the observed upregulation of CYP1A1 expression may indicate an increased risk of bioactivation of PAHs in fuels to harmful forms and later downstream health effects. In contrast, TNF-α, an inflammatory-related gene, was consistently downregulated in BEAS-2B cells. Suppression of TNF-α and other inflammatory biomarkers by PAHs have been previously reported [36, 59] and may be connected to a decreased ability to respond to cellular injury and pathogenesis of chronic inflammatory diseases [60].

Figure 7 demonstrates the correlation analysis between the responses in each toxicological assay and the chemical constituents of PM emissions. When analyzing the toxicological assays, DTT showed a moderate correlation with cytotoxicity (R = 0.67), which agrees with the results seen in either assay. However, DTT did not show a correlation with HMOX-1 expression, despite both DTT and HMOX-1 acting as indicators of oxidative potential. This discrepancy may be attributed to the presence of PM constituents that are capable of inducing oxidative injury but are not DTT active – as HMOX-1 expression was found to be moderately correlated with OC (R =0.39) – or endogenously ROS generated through cellular processes upon PM exposure [61]. The DTT assay is an isolated chemical reaction that can only measure exogenously generated ROS and the oxidative potential of PM constituents themselves. In contrast, gene expression analysis occurs in a complicated biological system where ROS may also be produced endogenously by various intracellular mechanisms. In addition, induction of HMOX-1 by PM constituents heavily depends on the bioavailability of the compound, which may depend on its water-solubility in cell culture media or interactions between organics and/or metals [61–63]. As a result, the DTT consumption of all fuels may not account for the total cellular oxidative stress when exposed to fuel PM. Interestingly, DTT showed a strong correlation with EC (R=0.85), which has been previously reported of not being redox active [64]. A recent study has also reported a notable correlation between DTT and EC, suggesting that EC provides the available surface area for reactions leading to superoxide formation [65].

Overall, the total PM mass was strongly correlated (R > 0.8) with both DTT activity and cytotoxicity in BEAS-2B cells. Total PM mass was also moderately anti-correlated with expression of TNF-α. Furthermore, the total mass of particle-phase PAHs for each fuel was moderately well correlated with DTT (R = 0.65) and strongly correlated with cytotoxicity (R = 0.94). When analyzing toxicological responses as functions of particle-phase PAH composition further, the DTT assay was found to be highly correlated with substituted PAHs and oxy-PAHs (R > 0.7), while cytotoxicity was strongly correlated with substituted, oxygenated, and non-substituted PAHs (R > 0.7). Previous studies have also shown good correlation between DTT activity and PAH emissions [64–66]. PAHs containing phenyl groups were not strongly correlated with either DTT or cytotoxicity, but did show moderate

Author Manuscript Author Manuscript Author Manuscript Author Manuscript

anti-correlations with CYP1A1 and HMOX-1 gene expression ($R < -0.5$) and strong anti-correlation with TNF-α ($R = -0.72$). Correlations between toxicological responses and individual PAHs detected in PM extracts can be found in Figure S1 (SM). It was observed that substituted two-ring PAHs (dimethyl- and methyl-naphthalenes), oxy-PAHs (i.e., xanthone, perinaphthenone, anthraquinone, 1,8-naphthalic anhydride), and three-ring PAHs (i.e., phenanthrene, pyrene, etc.) strongly correlated ($p \leq 0.05$) with DTT. Heavier four-member ring PAHs did not appear to correlate with DTT.

Metals emissions from the fuel blends were all, with the exception of Fe and Cu, moderately correlated with cytotoxicity ($R \geq 0.4$). Cu demonstrated a moderate anti-correlation with cytotoxicity ($R = -0.57$) and a moderate to weak anti-correlation with DTT activity, which agrees with previous studies that showed that the presence of Cu resulted in the suppression of DTT consumption [63]. DTT has also been found to form highly stable complexes with free Cu(I) [67]. Finally, Cu was the only metal to demonstrate a strong correlation with HMOX-1 gene expression ($R = 0.8$) and a moderate correlation with CYP1A1 ($R = 0.61$). These correlations may indicate increased activity of other enzymes that protect against ROS-mediated damage, such as the copper-zinc superoxide dismutase (SOD1), where Cu in the active site helps to catalyze the conversion of superoxide radicals to hydrogen peroxide [68–69]. Prior studies have demonstrated co-upregulation of CYP1A1 and SOD1 gene expression at both mRNA and protein levels after exposure to PAHs, such as benzo[a]pyrene [70–71].

4. Conclusions

This work investigated the emissions impacts and toxicity from a legacy off-road diesel engine when operated on R100 (or HVO) and biodiesel blends with R100 over the NRTC and D2 cycles. Results showed NOx emission benefits when utilizing R100 (statistically significant reductions ranged from 4.9%−5.4%), but NOx increases with increasing biodiesel blending in R100 (statistically significant increases ranged from 1.8%−4.2% only for R50/B50). PM mass showed large reductions for R100 and its blends with biodiesel compared to CARB ULSD, with larger reductions reported for the oxygenated fuel blends. These statistically significant reductions ranged from 38%−63% over the NRTC and from 27%−58% over the D2 cycle. Similar reductions were also observed for the total and solid particle number emissions. These results indicate that the use of aromatic and sulfur free fuels with or without the presence of oxygen will result in particulate emissions reductions from uncontrolled off-road engines. Carbonyl emissions did not show any significant fuel effects for either the NRTC or the D2 cycles. Trends toward lower carbonyl emissions were seen for the biodiesel blends compared to CARB ULSD. PAH emissions were measured in both the vapor- and particle-phase and dominated by low molecular weight species for all test fuels. Heavier PAHs were also detected in the particle-phase, but in lesser amounts, whereas they were undetectable in the vapor-phase due to their lower vapor pressure. For both phases, PAH emissions were lower for R100 and its blends with biodiesel. Nitrated PAH emissions were found in significantly lower concentrations than their parent PAHs, with mixed trends between the fuels.

Author Manuscript Author Manuscript Author Manuscript Author Manuscript

Our results showed that PM emissions from all fuels demonstrated the potential to induce oxidative damage when exposed to a cellular system. However, the use of biomass-derived fuels will likely decrease the oxidative stress in PM emissions, with the more oxygenated fuels providing greater reductions. Similar findings were observed in cytotoxicity of PM emissions. The increased upregulation of CYP1A1 may indicate an increased risk of bioactivation of PAHs for different fuels. PM emissions exhibited notable correlations with both DTT activity and cytotoxicity in BEAS-2B cells, whereas DTT moderately correlated with particle-phase PAH emissions. Some correlations were seen between DTT and trace elements/metals, but not with the redox active transition metals. The observed mixed effects may imply a dual role for metals that cause oxidative damage but also increased activity of other enzymes that protect against ROS-mediated damage.

Supplementary Material

Refer to Web version on PubMed Central for supplementary material.

Acknowledgements

We acknowledge funding from South Coast Air Quality Management District (SCAQMD) Contract No. 192082 and from the California Air Recourses Board CARB) under Contract No. 18ISD027. We acknowledge the National Biodiesel Board (NBB) and Renewable Energy Group, Inc., for providing test fuels as an in-kind contribution. Alexa Canchola was supported by an NRSA T32 training grant (T32 ES018827). We acknowledge Mr. Mark Villela, Mr. Victor Moran, and Mr. Daniel Gomez of the University of California, Riverside for performing the emissions testing.

References

1. Dallmann TR, Harley RA Evaluation of mobile source emission trends in the United States. J. Geophys. Res 2010, 115, D14305.
2. McCaffery C, Zhu H., Tang T, Li C, Karavalakis G, Cao S, Oshinuga A, Burnette A, Johnson KC, Durbin TD Real-world NOx emissions from heavy-duty diesel, natural gas, and diesel hybrid electric vehicles of different vocations on California roadways. Science of the Total Environment 2021, 784, 147224. [PubMed: 33905931]
3. Wang B, Lau Y-S, Huang Y, Organ B, Chuang H-C, Sai S, Ho SH, Qu L, Lee S-C, Ho K-F Chemical and toxicological characterization of particulate emissions from diesel vehicles. Journal of Hazardous Materials 2021, 405, 124613. [PubMed: 33301973]
4. Hart JE, Laden F, Schenker MB, Garshick E Chronic obstructive pulmonary disease mortality in diesel-exposed railroad workers. Environmental Health Perspectives 2006, 114, 1013–1017. [PubMed: 16835052]
5. Thurston GD, Kipen H, Annesi-Maesano I, Balmes J, Brook RD, Cromar K, De Matteis S, Forastiere F, Forsberg B, Frampton MW, Grigg J, Heederik D, Kelly FJ, Kuenzli N, Laumbach R, Peters A, Rajagopalan ST, Rich D, Ritz B, Samet JM, Sandstrom T, Sigsgaard T, Sunyer J, Brunekreef B A joint/ATS policy statement: what constitutes an adverse health effect of air pollution? An analytical framework. European Respiratory Journal 2017, 49, 1600419. [PubMed: 28077473]
6. Preble CV, Dallmann TR, Kreisberg NM, Hering SV, Harley RA, Kirchstetter TW Effects of particle filters and selective catalytic reduction on heavy-duty diesel drayage truck emissions at the Port of Oakland. Environ. Sci. Technol 2015, 49, 8864–8871. [PubMed: 26083075]
7. Preble CV, Cados TE, Harley RA, Kirchstetter TW In-use performance and durability of particle filters on heavy-duty diesel trucks. Environ. Sci. Technol 2018, 52, 11913–11921. [PubMed: 30153019]
8. Haugen MJ, Bishop GA Long-term fuel-specific NOx and particle emission trends for in-use heavy-duty vehicles in California. Environ. Sci. Technol 2018, 52, 6070–6076. [PubMed: 29692175]

Author Manuscript Author Manuscript Author Manuscript Author Manuscript

9. Kean AJ, Sawyer RF, Harley RA A fuel-based assessment of off-road diesel engine emissions. J. Air Waste Manage. Assoc 2000, 50, 1929–1939.
10. Niemi S, Lundin K, Karhu T, Lauren M, Ekman K, Nousiainen P, Paanu T Exhaust particle number in off-road engines of different generations. SAE Technical Paper 2009, 2009-01-1869.
11. Cao T, Durbin TD, Russell RL, Cocker III DR, Scora G, Maldonado H, Johnson KC Evaluations of in-use emission factors from off-road construction equipment. Atmospheric Environment 2016, 147, 234–245.
12. Abolhasani S, Frey HC, Kim K, Rasdorf W, Lewis P, Pang S-H Real-world in-use activity, fuel use, and emissions for nonroad construction vehicles: A case study for excavators. J. Air Waste Manage. Assoc 2008, 58, 1033–1046.
13. Desouza CD, Marsh DJ, Beevers SD, Molden N, Green DC A spatial and fleet disaggregated approach to calculating the NOx emissions inventory from non-road mobile machinery in London. Atmospheric Environment: X 2021, 12, 100125.
14. Van Gerpen J Biodiesel processing and production. Fuel Processing Technology 2005, 86, 1097–1107.
15. Karavalakis G, Johson KC, Hajbabaei M, Durbin TD Application of low-level biodiesel blends on heavy-duty (diesel) engines: feedstock implications on NOx and particulate emissions. Fuel 2016, 151, 259–268.
16. Na K, Biswas S, Robertson W, Sahay K, Okamoto R, Mitchell A, Lemieux S Impact of biodiesel and renewable diesel on emissions of regulated pollutants and greenhouse gases on a 2000 heavy duty diesel truck. Atmospheric Environment 2015, 107, 307–314.
17. Fontaras G, Karavalakis G, Kousoulidou M, Tzamkiozis T, Ntziachristos L, Bakeas E, Stournas S, Samaras Z Effects of biodiesel on passenger car fuel consumption, regulated and non-regulated pollutant emissions over legislated and real-world driving cycles. Fuel 2009, 88, 1608–1617.
18. Eckerle WA, Lyford-Pike EJ, Stanton DW, LaPointe LA, Whitacre SD, Wall JC Effects of methyl ester biodiesel on NOx emissions. SAE Technical Paper 2008, 2008-01-0078.
19. Mueller C, Boehman A, Martin G An experimental investigation of the origin of increased NOx emissions when fueling a heavy-duty compression-ignition engine with soy biodiesel. SAE International Journal of Fuels and Lubricants 2009, 2, 789–816.
20. Karavalakis G, Boutsika V, Stournas S, Bakeas E Biodiesel emissions profile in modern diesel vehicles. Part 2: Effect of biodiesel origin on carbonyl, PAH, nitro-PAH and oxy-PAH emissions. Science of the Total Environment 2011, 409, 738–747. [PubMed: 21122895]
21. Karavalakis G, Gysel N, Schmitz DA, Cho AK, Sioutas C, Schauer JJ, Cocker DR, Durbin TD Impact of biodiesel on regulated and unregulated emissions, and redox and proinflammatory properties of PM emitted from heavy-duty vehicles. Science of the Total Environment 2017, 584–585, 1230–1238.
22. Martin N, Lombard M, Jensen KR, Kelly P, Pratt T, Travis N Effect of biodiesel fuel on ‘real-world’, nonroad heavy duty diesel engine particulate matter emissions, composition and cytotoxicity. Science of the Total Environment 2017, 586, 409–418. [PubMed: 28236480]
23. Tsai J-H, Chen S-J, Lin S-L, Huang KL, Hsueh CK, Lin C-C, Li P-M Emissions of PM2.5-Bound Polycyclic Aromatic Hydrocarbons and Metals from a Diesel Generator Fueled with Biodiesel Converted from Used Cooking Oil. Aerosol and Air Quality Research, 2019, 19, 1555–1565.
24. Hartikka TM, Kuronen M, Kiiski U Technical performance of HVO (hydrotreated vegetable oil) in diesel engines. SAE Technical Paper 2012, 2012-01-1585.
25. Singh D, Subramanian KA, Garg MO Comprehensive review of combustion, performance and emissions characteristics of a compression ignition engine fueled with hydroprocessed renewable diesel. Renewable and Sustainable Energy Reviews 2018, 81, 2947–2954.
26. Happonen M, Heikkila J, Murtonen T, Lehto K, Sarjovaara T, Larmi M, Keskinen J, Virtanen A Reductions in particle and NOx emissions by diesel engine parameter adjustments with HVO fuel. Environ. Sci. Technol 2012, 46, 6198–6204. [PubMed: 22568591]
27. Heikkila J, Happonen M, Murtonen T, Lehto K, Sarjovaara T, Larmi M, Keskinen J, Virtanen A Study of Miller timing on exhaust emissions of a hydrotreated vegetable oil (HVO)-fueled diesel engine. J. Air Waste Manage. Assoc 2012, 62, 1305–1312.

Author Manuscript Author Manuscript Author Manuscript Author Manuscript

28. Murtonen T, Aakko-Saksa P, Kuronen M, Mikkonen S, Lehtoranta K Emissions with heavy-duty diesel engines and vehicles using FAME, HVO and GTL fuels with and without DOC+POC aftertreatment. SAE International Journal of Fuels and Lubricants 2010, 2, 147–166.
29. Bugarski AD, Hummer JA, Vanderslice S Effects of hydrotreated vegetable oil on emissions of aerosols and gases from light-duty and medium-duty older technology engines. J. Occup. Environ. Hyg 2016, 13, 297–306.
30. Pirjola L, Ronkko T, Saukko E, Parviainen H, Malinen A, Alanen J, Saveljeff H Exhaust emissions of non-road mobile machine: Real-world and laboratory studies with diesel and HVO fuels. Fuel 2017; 202, 154–164.
31. Murtonen T, Aakko-Saksa P, Koponen P, Lehto K, Sarjovaara T, Happonen M, Keikkila J Emission reduction potential with paraffinic renewable diesel by optimizing engine settings or using oxygenate. SAE Technical Paper 2012, 2012-01-1590.
32. Vojtisek-Lom M, Beranek V, Mikuska P, Krumal K, Coufalik P, Sikorova J, Topinka J Blends of butanol and hydrotreated vegetable oils a drop-in replacement for diesel engines: Effects on combustion and emissions. Fuel 2017, 197, 407–421.
33. Westphal GA, Krahl J, Munack A, Rosenkranz N, Schroder O, Schaak J, Pabst C, Bruning T, Bunger J Combustion of hydrotreated vegetable oil and jatropha methyl ester in a heavy duty engine: Emissions and bacterial mutagenicity. Environ. Sci. Technol 2013, 47, 6038–6046. [PubMed: 23647143]
34. Prokopowicz A, Zaciera M, Sobczak A, Bielaczyc P, Woodburn J The effects of neat biodiesel and biodiesel and HVO blends in diesel fuel on exhaust emissions from a light duty vehicle with a diesel engine. Environ. Sci. Technol 2015, 49, 7473–7482. [PubMed: 25993509]
35. Cocker DR, Shah S, Johnson K, Miller JW, Norbeck J Development and application of a mobile laboratory for measuring emissions from diesel engines. I regulated gaseous emissions. Environ. Sci. and Technol 2004, 38, 2182–2189. [PubMed: 15112823]
36. Ahmed CMS, Yang J, Chen JY, Jiang H, Cullen C, Karavalakis G, Lin Y-H Toxicological responses in human airway epithelial cells (BEAS-2B) exposed to particulate matter emissions from gasoline fuels with varying aromatic and ethanol levels. Science of The Total Environment 2020, 706, 135732. [PubMed: 31818575]
37. Glaude PA, Fournet R, Bounaceur R, Moliere M Adiabatic flame temperature from biofuels and fossil fuels ad derived effect on NOx emissions. Fuel Process Technol 2010, 91, 229–235.
38. Hellier P, Talibi M, Eveleigh A, Ladommatos N An overview of the effects of fuel molecular structure on the combustion and emissions characteristics of compression ignition engines. Proceedings of the Institution of Mechanical Engineers, Part D: Journal of Automobile Engineering 2017, 232, 90–105.
39. Bhardwaj O, Kolbeck AF, Kkoerfer T, Honkanen M Potential of hydrogenated vegetable oil (HVO) in future high efficiency combustion system. SAE Int. J. Fuels Lubr 2013, 63, 157–169.
40. Flynn PF, Durrett RP, Hunter GL, zur Loye AO, Akinyemi OC, Dec JE, Westbrook CK. Diesel combustion: An integrated view combining laser diagnostics, chemical kinetics, and empirical validation. SAE Technical Paper 1999, 1999-01-0509.
41. Sun W, Wang Q, Guo L, Cheng P, Li D, Yan Y Influence of biodiesel/diesel blends on particle size distribution of CI engine under steady/transient conditions. Fuel 2019, 245, 336–344.
42. Cahill TM, Okamoto RA Emissions of acrolein and other aldehydes from biodiesel-fueled heavy-duty vehicles. Environ. Sci. Technol 2012, 46, 8382–8388. [PubMed: 22746209]
43. Zervas E Regulated and non-regulated pollutants emitted from two aliphatic and commercial diesel fuel. Fuel 2008, 87, 1141–1147.
44. Cho AK, Di Stefano E, You Y, Rodriguez CE, Schmitz AD, Kumagai Y, Miguel AH, Eiguren-Fernandez A, Kobayashi T, Froines JR Determination of four quinones in diesel exhaust particles, SRM 1649a, and atmospheric PM2.5. Aerosol Science and Technology 2004, 38, 68–81.
45. Chu H, Shang J, Lin M, Chen Y, Pan Y, Li Y, Tao Y, Cheng Z, Meng Q, Li Q, Jia G, Zhu T, Hao W, Wei X Comparison of lung damage in mice exposed to black carbon particles and 1,4-naphthoquinone coated black carbon particles. Science of the Total Environment 2017, 580, 572–581. [PubMed: 28034545]

Author Manuscript Author Manuscript Author Manuscript Author Manuscript

46. Liu ZG, Wall JC, Ottinger NA, McGuffin D Mitigation of PAH and nitro-PAH emissions from nonroad diesel engines. Environ. Sci. Technol 2015, 49, 3662–3671. [PubMed: 25668360]
47. Khalek I, Bougher T, Merritt P Regulated and unregulated emissions from highway heavy-duty diesel engines complying with U.S. Environmental Protection Agency 2007 Emissions Standards. J. Air Waste Manage. Assoc 2011, 61, 427–442.
48. Lea-Langton A, Li H, Andrews GE Comparison of particulate PAH emissions for diesel, biodiesel and cooking oil using a heavy duty DI diesel engine. SAE Technical Paper 2008, 2008-01-1811.
49. Karavalakis G, Fontaras G, Ampatzoglou D, Kousoulidou M, Stournas S, Samaras Z, Bakeas E Effects of low concentration biodiesel blends application on modern passenger cars. Part 3: Impact on PAH, nitro-PAH, and oxy-PAH emissions. Environmental Pollution 2010, 158, 1584–1594. [PubMed: 20083330]
50. Li Q, Wyatt A, Kamens RM Oxidant generation and toxicity enhancement of aged-diesel exhaust. Atmospheric Environment 2009, 43, 1037–1042.
51. Gerlofs-Nijland ME, Totlandsdal AI, Tzamkiozis T, Leseman DLAC, Samaras Z, Låg M, Schwarze P, Ntziachristos L, Cassee FR Cell toxicity and oxidative potential of engine exhaust particles: impact of using particulate filter or biodiesel fuel blend. Environ. Sci. Technol 2013, 47, 5931–5938. [PubMed: 23597117]
52. Holmen BA, Rukavina B, Kasumba J, Fukagawa NK Reactive oxidative species and speciated particulate light-duty engine emissions from diesel and biodiesel fuel blends. Energy and Fuels 2017, 31, 8171–8180.
53. Jalava PI, Aakko-Saksa P, Murtonen T, Happo MS, Markkanen A, Yli-Pirilä P, Hakulinen P, Hillamo R, Maki-Paakkanen J, Salonen RO, Jokiniemi J, Hirvonen M-R Toxicological properties of emission particles from heavy duty engines powered by conventional and bio-based diesel fuels and compressed natural gas. Part. Fibre Toxicol 2012, 9, 37. [PubMed: 23021308]
54. Botero ML, Mendoza C, Arias S, Hincapie OD, Agudelo JR, Ortiz IC In vitro evaluation of the cytotoxicity and DNA damage induced by particle matter and gaseous emissions from a medium-duty diesel vehicle under real driving condition using palm oil biodiesel blends. Environmental Pollution 2020, 265, Part A, 115034. [PubMed: 32806412]
55. Iso, I. S. O. 2009. "10993–5: 2009 Biological evaluation of medical devices—part 5: tests for in vitro cytotoxicity." International Organization for Standardization, Geneva.
56. Livak KJ, Schmittgen TD Analysis of Relative Gene Expression Data Using Real-Time Quantitative PCR and the 2−ΔΔCT Method. Methods 2001, 25, 402–408. [PubMed: 11846609]
57. Gozzelino R, Viktoria J, Soares MP Mechanisms of Cell Protection by Heme Oxygenase-1. Annual Review of Pharmacology and Toxicology 2010, 50, 323–354.
58. Zhou S-F, Liu J-P, Chowbay B Polymorphism of human cytochrome P450 enzymes and its clinical impact. Drug Metabolism Reviews 2009, 41, 89–295. [PubMed: 19514967]
59. Manzano-León N, Serrano-Lomelin J, Sánchez BN, Quintana-Belmares R, Vega E, Vázquez-López I, Rojas-Bracho L, López-Villegas MT, Vadillo-Ortega F, De Vizcaya-Ruiz A TNF α and IL-6 responses to particulate matter in vitro: variation according to PM size, season, and polycyclic aromatic hydrocarbon and soil content. Environmental Health Perspectives 2016, 124, 406–412. [PubMed: 26372663]
60. Park K, Lee J-H, Cho H-C, Cho S-Y, Cho J-W Down-regulation of IL-6, IL-8, TNF-α and IL-1β by glucosamine in HaCaT cells, but not in the presence of TNF-α. Oncology Letters 2010, 1, 289–292. [PubMed: 22966296]
61. Jiang H, Ahmed CM, Canchola A, Chen JY, Lin Y-H Use of dithiothreitol assay to evaluate the oxidative potential of atmospheric aerosols. Atmosphere 2019, 10, 571.
62. Dou J, Lin P, Kuang B-Y, Yu JZ Reactive oxygen species production mediated by humic-like substances in atmospheric aerosols: enhancement effects by pyridine, imidazole, and their derivatives. Environ. Sci. Technol 2015, 49, 6457–6465. [PubMed: 25961507]
63. Yu H, Wei J, Cheng Y, Subedi K, Verma V Synergistic and antagonistic interactions among the particulate matter components in generating reactive oxygen species based on the dithiothreitol assay. Environ. Sci. Technol 2018, 52, 2261–2270. [PubMed: 29351719]

Author Manuscript Author Manuscript Author Manuscript Author Manuscript

64. Cho AK, Sioutas C, Miguel AH, Kumagai Y, Schmitz DA, Singh M, Eiguren-Fernandez A, Froines JR Redox activity of airborne particulate matter at different sites in the Los Angeles Basin. Environmental Research 2005, 99, 40–47. [PubMed: 16053926]

65. Saffari A, Daher N, Shafer MM, Schauer JJ, Sioutas C Seasonal and spatial variation in dithiothreitol (DTT) activity of quasi-ultrafine particles in the Los Angeles Basin and its association with chemical species. Journal of Environmental Science and Health, Part A 2014, 49, 441–451.

66. Li N, Sioutas C, Cho A, Schmitz D, Misra C, Sempf J, Wang M, Oberley T, Froines J, Nel A Ultrafine particulate pollutants induce oxidative stress and mitochondrial damage. Environ. Health Perspect 2003, 111, 455–460. [PubMed: 12676598]

67. Krężel A, Leśniak W, Jeżowska-Bojczuk M, Młynarz P, Brasuñ J, Kozłowski H, Bal W Coordination of heavy metals by dithiothreitol, a commonly used thiol group protectant. Journal of Inorganic Biochemistry 2001, 84, 77–88. [PubMed: 11330484]

68. Franco MC, Dennys CN, Rossi FH, Estévez AG Superoxide dismutase and oxidative stress in amyotrophic lateral sclerosis. Chapter 5 in Current Advances in Amyotrophic Lateral Sclerosis 2013, ed. Estévez A (London: IntechOpen).

69. Tainer JA, Getzoff ED, Richardson JS, David C Richardson. Structure and mechanism of copper, zinc superoxide dismutase. Nature 1083, 306, 284–287.

70. Marshall K, Liu Z, Olfert IM, Gao W Chronic electronic cigarette use elicits molecular changes related to pulmonary pathogenesis. Toxicology and Applied Pharmacology 2020, 406, 115224. [PubMed: 32890605]

71. Lin S, Ren A, Wang L, Huang Y, Wang Y, Wang C, Greene ND Oxidative Stress and Apoptosis in Benzo[a]pyrene-Induced Neural Tube Defects. Free Radical Biology and Medicine 2018, 116, 149–158. [PubMed: 29309894]

Author Manuscript Author Manuscript Author Manuscript Author Manuscript

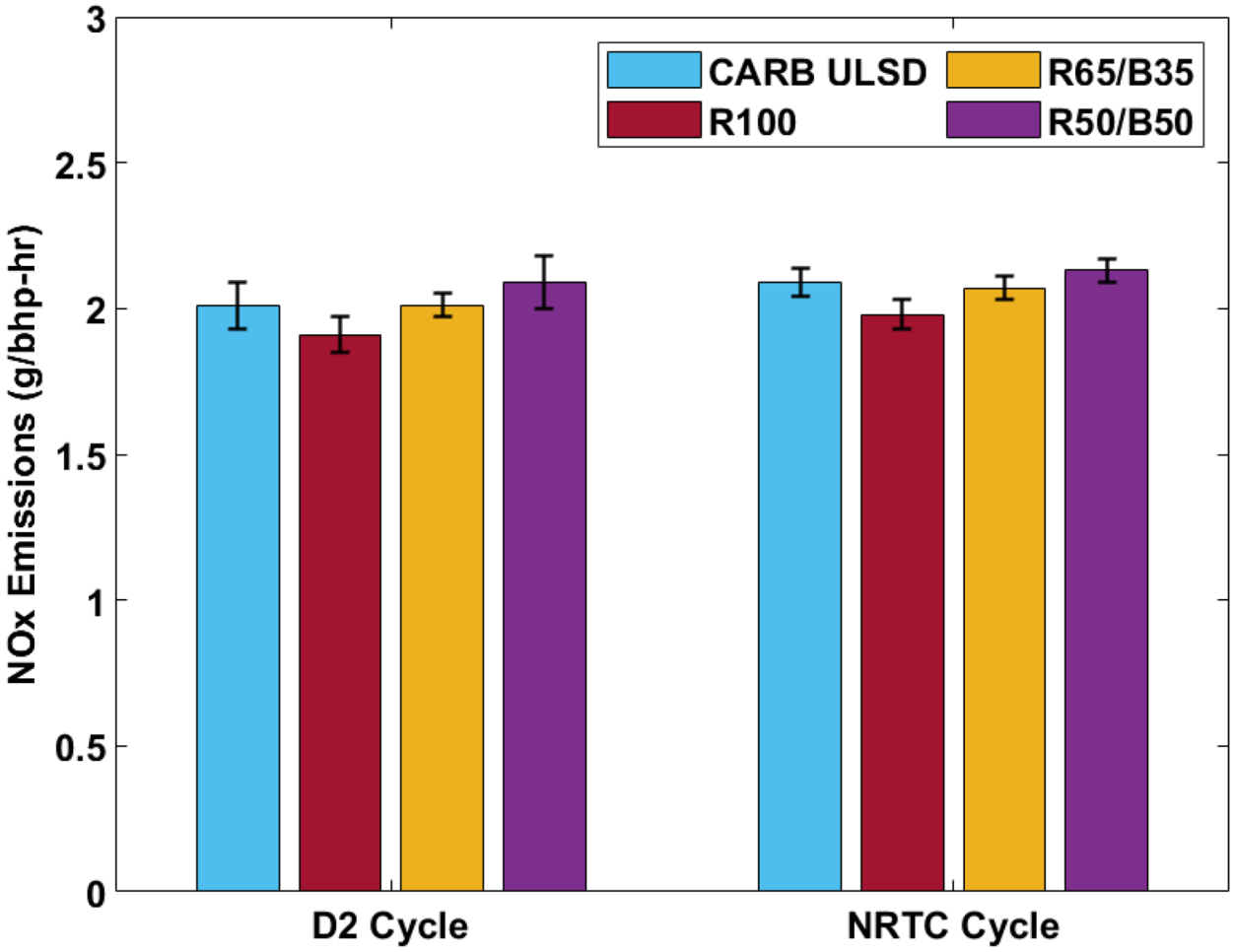

Figure 1:
NOx emissions, expressed in g/bhp-hr, for all fuels over the D2 and NRTC test cycles

Author Manuscript Author Manuscript Author Manuscript Author Manuscript

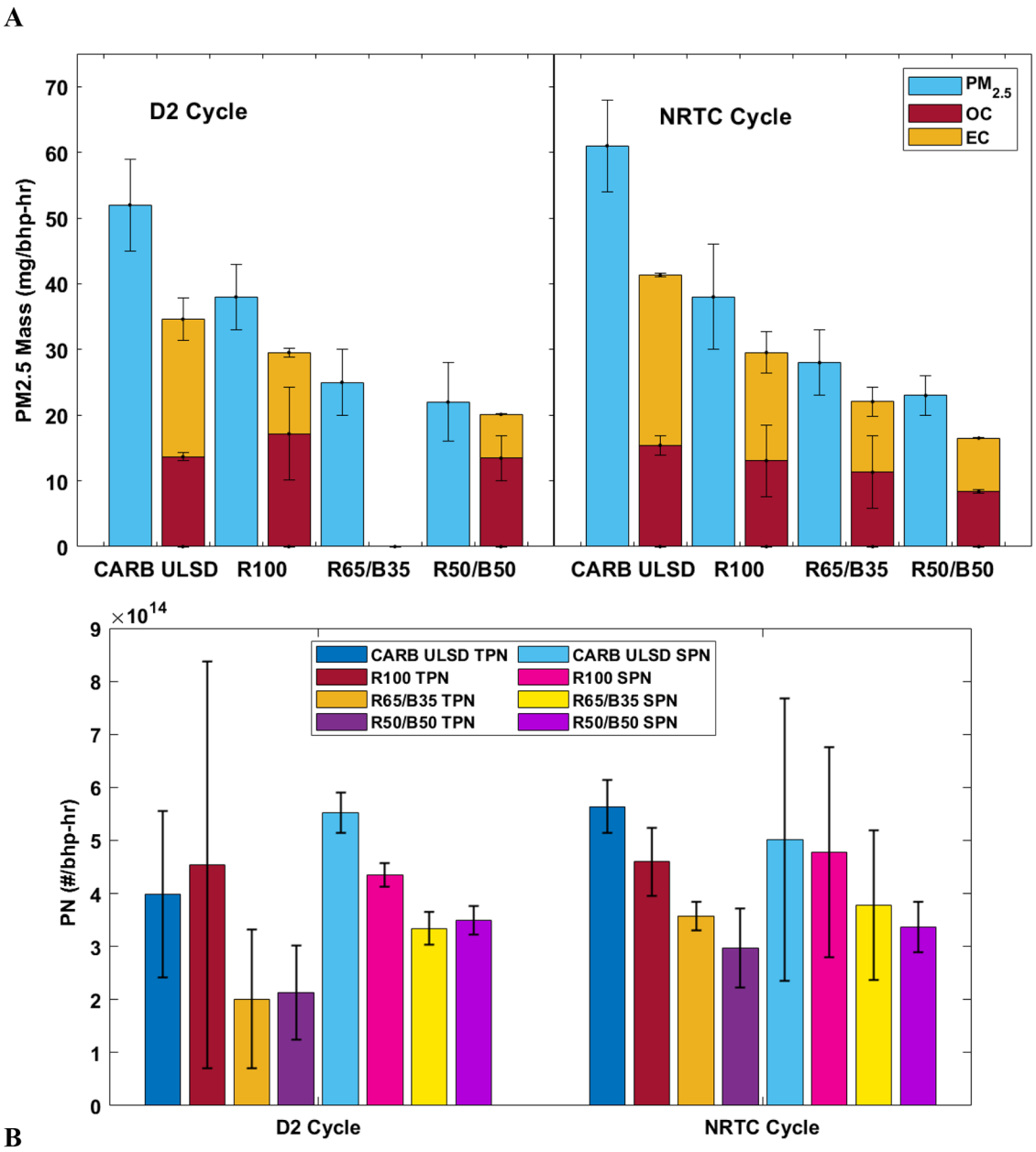

Figure 2 (a-b):
PM mass and EC/OC fractions (top panel), and total (volatile and solid) and solid particle number (above 23 nm) emissions (bottom panel) for all fuels over the D2 and NRTC test cycles

Author Manuscript Author Manuscript Author Manuscript Author Manuscript

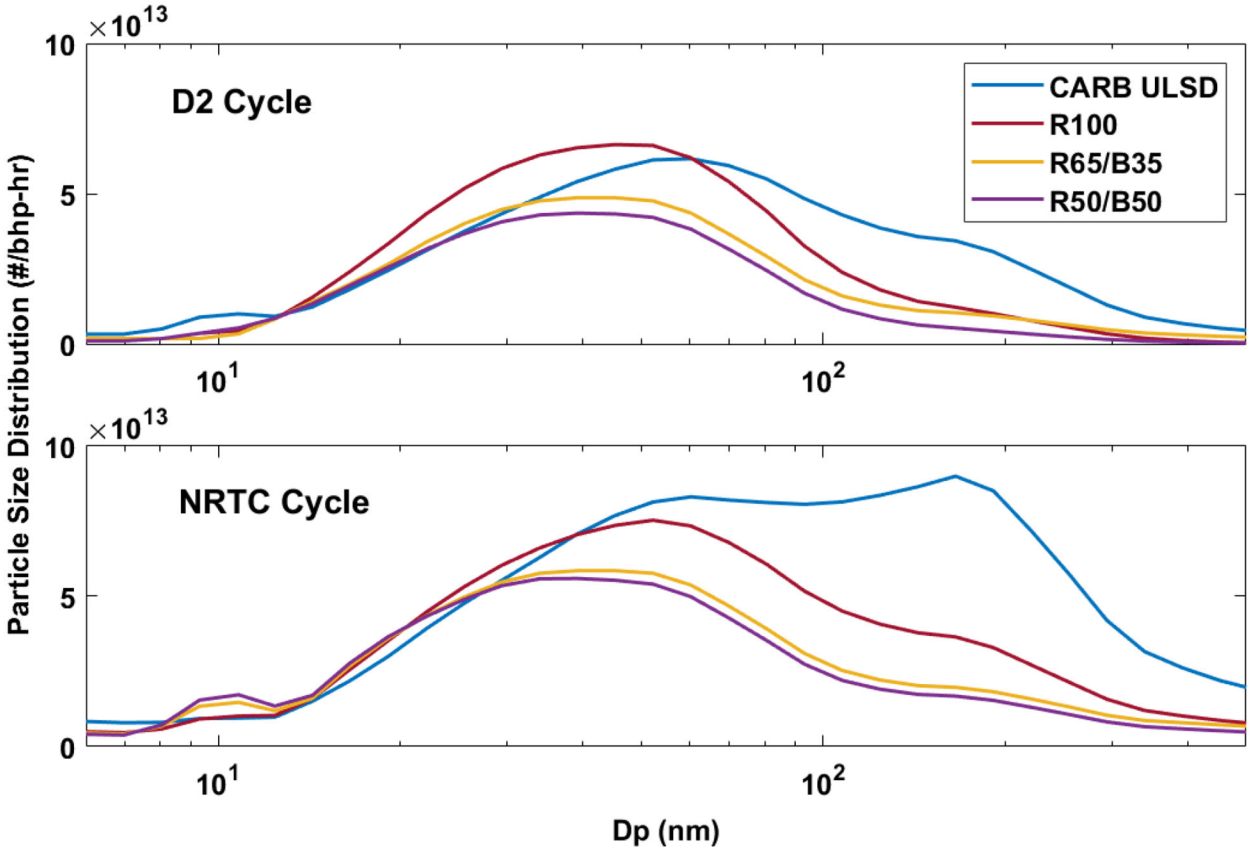

Figure 3:
Particle size distributions for all fuels over the D2 (top panel) and NRTC (bottom panel) test cycles

Author Manuscript Author Manuscript Author Manuscript Author Manuscript

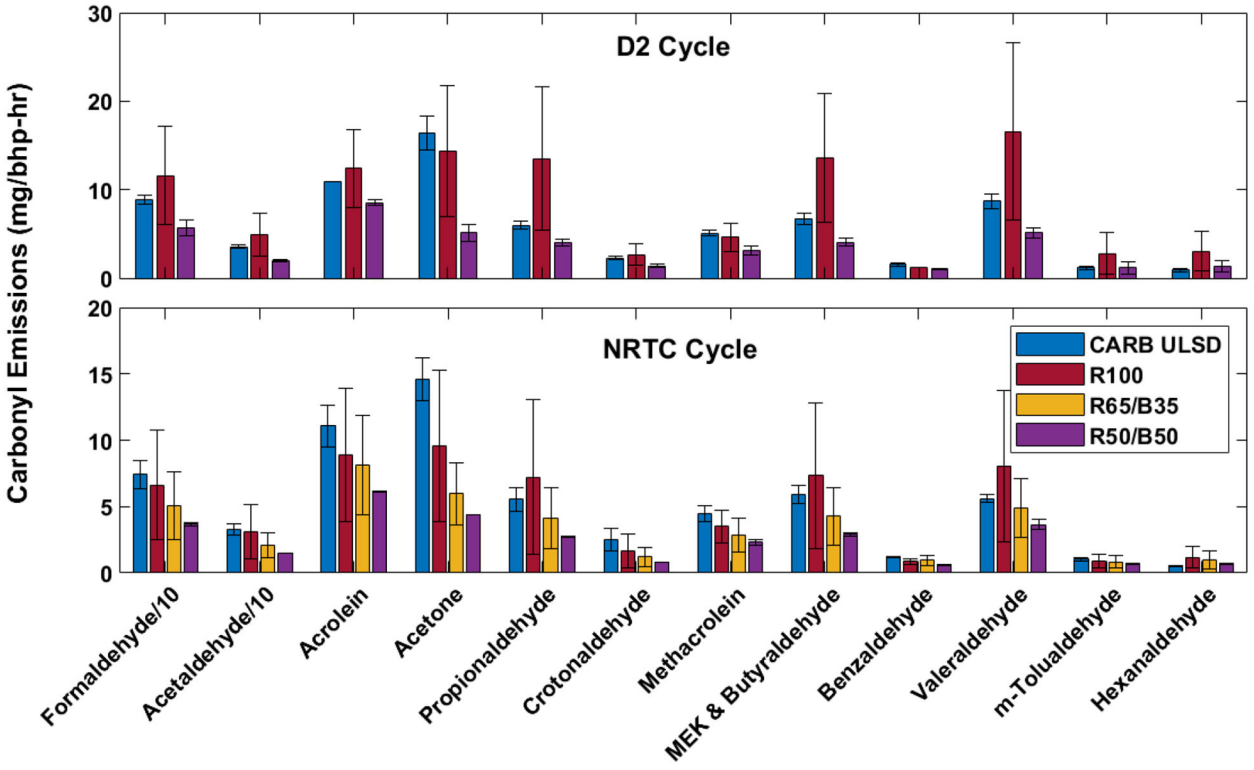

Figure 4:
Carbonyl emissions for all fuels over the D2 (top panel) and NRTC (bottom panel) test cycles; Note than formaldehyde and acetaldehyde emissions are divided by a factor of 10

Author Manuscript Author Manuscript Author Manuscript Author Manuscript

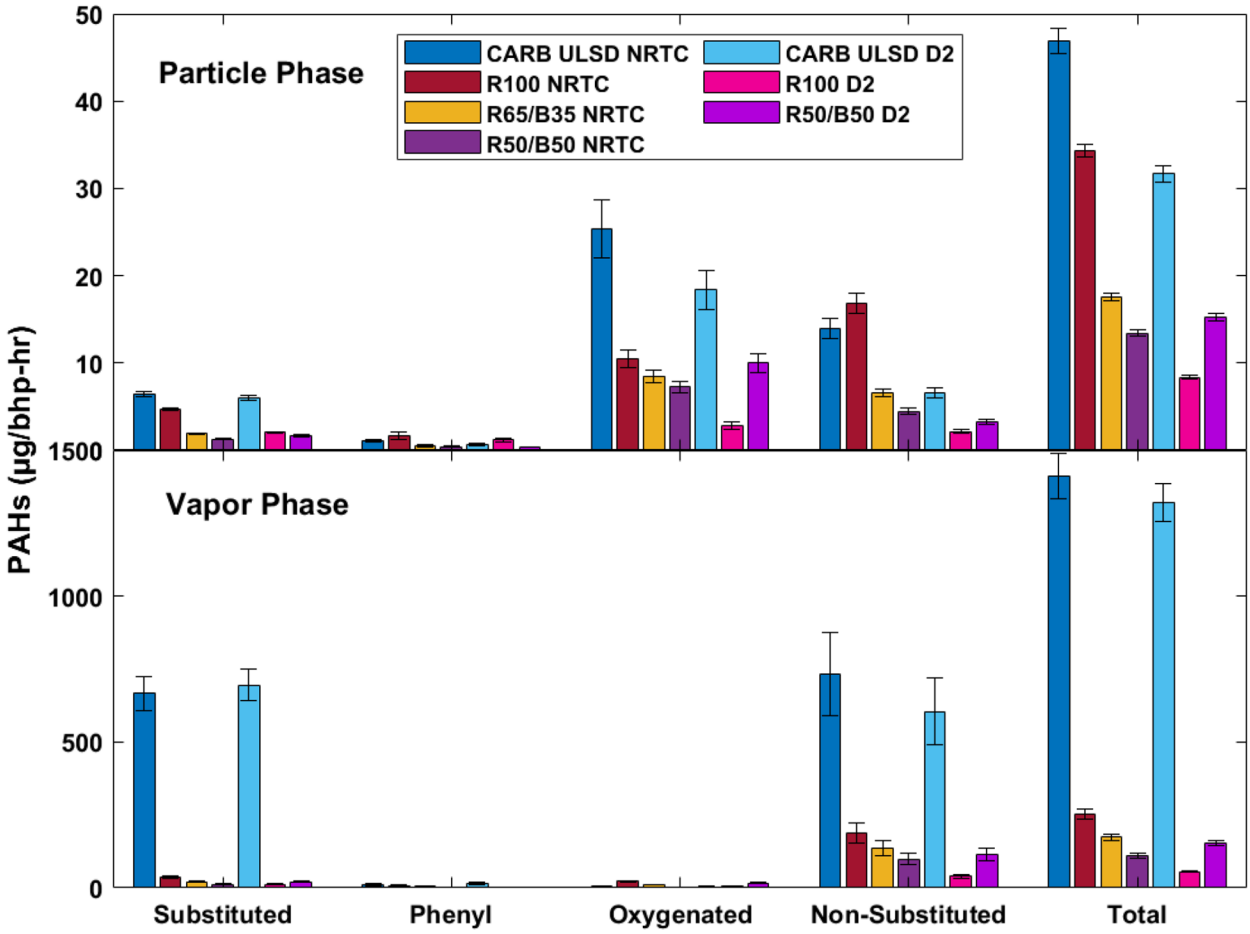

Figure 5:

Substituted, phenyl, oxygenated, non-substituted, and total PAH emissions in the particle-phase (top panel) and vapor-phase (bottom panel) for all fuels over the D2 and NRTC test cycles

Author Manuscript Author Manuscript Author Manuscript Author Manuscript

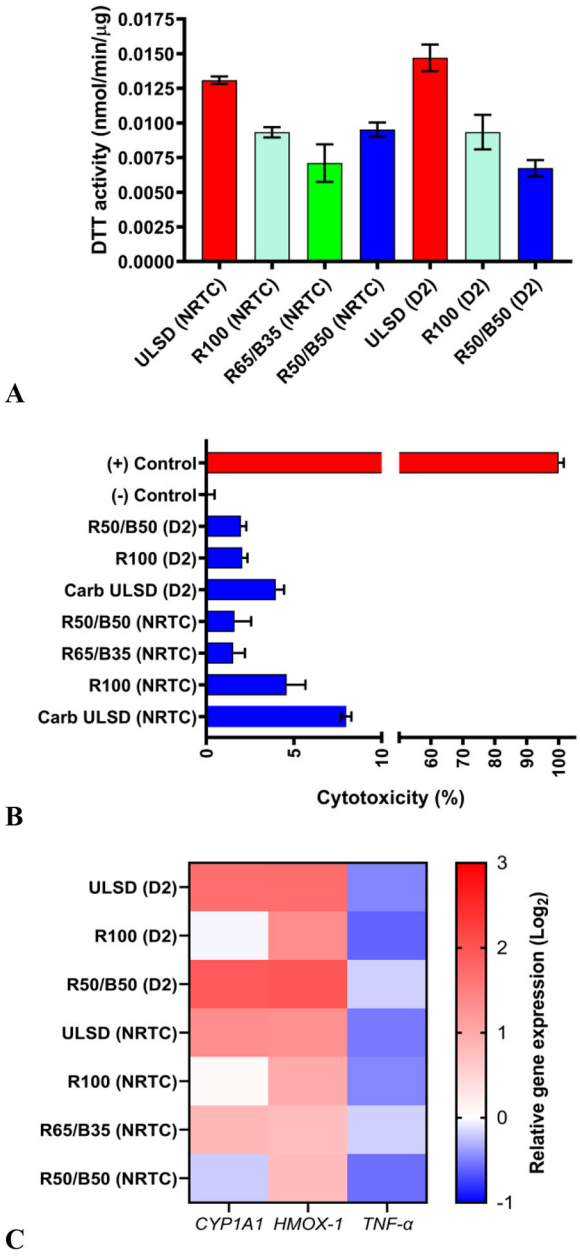

Figure 6 (a-c):

Toxicological characterization of PM emissions for all fuels over the D2 and NRTC test cycles; (a) DTT activity (nmol/min/µg) of PM, (b) Cytotoxicity of PM exposed to BEAS-2B cells and expressed as percentage of lactate dehydrogenase (LDH) release relative to negative controls of unexposed cells and positive controls treated with Triton X-100 (0.1%v/v), and (c) Differential gene expression of CYP1A1, HMOX-1, and TNF-α in BEAS-2B cells after 24 h exposure to PM extracts. Results are expressed as the fold change (log_2) over unexposed controls and normalized to a housekeeping gene (ACTB). Positive and negative values represent upregulation and downregulation of biomarkers, respectively

Author Manuscript Author Manuscript Author Manuscript Author Manuscript

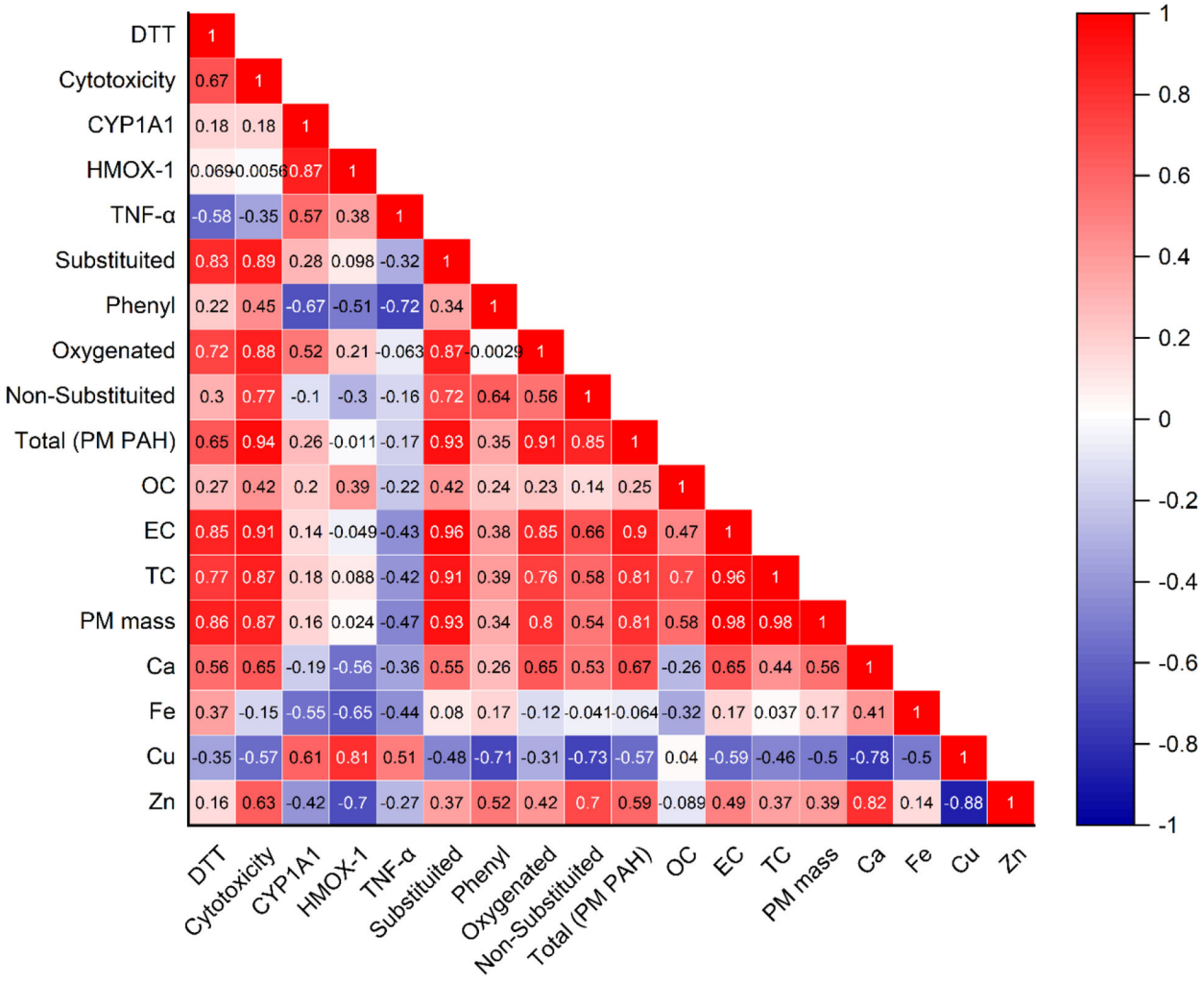

Figure 7:

Correlation matrix for individual pollutants, DTT activity, cytotoxicity, and biomarker responses. Positive correlations are depicted in red, while negative correlations are depicted in blue

Author Manuscript

Author Manuscript

Author Manuscript

Author Manuscript

Table 1:

Metals and trace elements, expressed in μg/bhp-hr, for all fuels and test cycles

	D2 Cycle			NRTC Cycle			
	CARB ULSD	**R100**	**R50/B50**	**CARB ULSD**	**R100**	**R65/B35**	**R50/B50**
Na	110.8 ± 34.3	71.7 ± 57.7	83.3 ± 20.5	427.1 ± 203.5	268.7 ± 37.9	251.9 ± 6.5	230.6 ± 106.9
Si	11.2 ± 2.9	8.3 ± 10.0	6.0 ± 5.7	11.2 ± 1.0	11.0 ± 4.6	9.1 ± 1.2	11.4 ± 7.3
P	14.8 ± 3.1	8.2 ± 3.1	9.2 ± 0.7	15.7 ± 8.2	15.2 ± 6.0	13.5 ± 1.1	14.0 ± 0.6
S	16.0 ± 3.6	13.0 ± 2.2	14.1 ± 0.3	53.5 ± 35.0	32.6 ± 14.2	41.0 ± 4.9	42.6 ± 12.6
Cl	11.3 ± 3.6	2.3 ± 1.2	9.3 ± 2.6	57.7 ± 61.5	25.1 ± 4.8	30.2 ± 16.0	34.7 ± 23.0
Ca	12.1 ± 6.6	6.6 ± 2.4	4.8 ± 0.5	19.1 ± 10.6	11.7 ± 5.2	12.6 ± 1.7	14.6 ± 5.1
Fe	10.0 ± 7.1	8.3 ± 4.6	2.9 ± 0.7	6.6 ± 4.6	7.8 ± 3.6	9.6 ± 0.3	9.8 ± 5.5
Cu	3.4 ± 0.8	3.2 ± 4.1	6.0 ± 2.1	0.9 ± 1.3	1.0 ± 1.4	2.3 ± 1.9	2.5 ± 2.1
Zn	16.4 ± 3.2	20.4 ± 0.1	14.4 ± 0.0	41.5 ± 39.3	32.8 ± 1.8	30.2 ± 5.9	28.3 ± 12.2